J Membrane Biol (2011) 239:167–175
DOI 10.1007/s00232-010-9335-5

TEA-Sensitive Currents Contribute to Membrane Potential of Organ Surface Primo-node Cells in Rats

Jae-Hong Choi · Chae Jeong Lim · Tae Hee Han · Seul Ki Lee · So Yeong Lee · Pan Dong Ryu

Received: 3 September 2010 / Accepted: 16 November 2010 / Published online: 14 December 2010

Abstract The primo-vascular (Bonghan) tissue has been identified in most tissues in the body, but its structure and functions are not yet well understood. We characterized electrophysiological properties of the cells of the primo-nodes (PN) on the surface of abdominal organs using a slice patch clamp technique. The most abundant were small round cells ($\sim$10 μm) without processes. These PN cells exhibited low resting membrane potential (−36 mV) and did not fire action potentials. On the basis of the current–voltage (I–V) relationships and kinetics of outward currents, the PN cells can be grouped into four types. Among these, type I cells were the majority (69%); they showed strong outward rectification in I–V relations. The outward current was activated rapidly and sustained without decay. Tetraethylammonium (TEA) dose-dependently blocked both outward and inward current (IC_{50}, 4.3 mM at ±60 mV). In current clamp conditions, TEA dose-dependently depolarized the membrane potential (18.5 mV at 30 mM) with increase in input resistance. The tail current following a depolarizing voltage step was reversed at −27 mV, and transient outward current like A-type K^+ current was not expressed at holding potential of −80 mV. Taken together, the results demonstrate for the first time that the small round PN cells are heterogenous, and that, in type I cells, TEA-sensitive current with limited selectivity to K^+ contributed to resting membrane potential of these cells.

J.-H. Choi · C. J. Lim · T. H. Han · S. K. Lee · S. Y. Lee · P. D. Ryu (✉)
Laboratory of Veterinary Pharmacology, Research Institute of Veterinary Science, College of Veterinary Medicine, Seoul National University, 599 Gwanak-Ro, Gwanak-Gu, Seoul 151-742, Republic of Korea
e-mail: pdryu@snu.ac.kr

Keywords Primo-vascular system · Bonghan tissue · Slice patch clamp · Input resistance · Input capacitance · Current–voltage relationship

The primo-vascular system (Bonghan system) is a network of novel threadlike tissues claimed as acupuncture meridians in the 1960s. It has been identified in many parts of the body including the surface of internal organs, the skin, the lymphatic vessels, blood vessels, the omentum, the central nervous system, and adipose tissues (see Soh 2009 for a review). The primo-vascular system is composed of the primo-vessels (PV) that connect the primo-nodes (PN), and primo-liquid that flows though the PVs (Soh 2009). PVs have bundle structures composed of 10-μm-thick subducts that are clearly different from blood or lymphatic capillaries (Lee et al. 2007; Ogay et al. 2009). Spherical DNA containing granules, so-called primo-micro cells 1.7–2.5 μm in diameter, flow through the ducts (Ogay et al. 2006).

Until now, understanding the anatomical and histological properties of these structures was the mainstay of primo-research, but their functions are not well understood. PNs (the Bonghan corpuscles) are reported to contain immune cells such as macrophages, mast cells, eosinophils, and basophils (Lee et al. 2007), suggesting an immune function for the primo-vascular system. The primo-vascular system also demonstrated a flow of dye to a distance up to 12 cm at 0.3 mm/s flow speed (Sung et al. 2008), a flow of cancer cells as a novel pathway for cancer metastasis (Yoo et al. 2009), and a flow of Alcian blue dye injected at the acupoint BL23 to the surface of abdominal organs (Han et al. 2009). In addition, proteomic analysis of tissues and liquid from PVs showed, by analyzing gene ontology to other proteins, that primo-vascular tissues were associated

with stem cells, especially mesenchymal stem cells, cancer cells, and myeloid cells (Lee et al. 2008). The primo-vascular system may represent niches for mesenchymal stem cells of macrophages in adipose tissues (Lee et al. 2009). These results imply that the primo-vascular system may play a role as a circulatory or conductive channel.

It has been reported that there were three types of spontaneous electrical activities in the primo-vascular tissues (Kim 1963). In a previous study, we also found that the cells in the PVs of organ surface primo-vascular tissues had a resting membrane potential (RMP) of −40 mV and spontaneous electrical activities (Park et al. 2009). However, little is known about the electrophysiological properties of the PN cells. In this study, we developed a slice preparation procedure for PNs and characterized the basic electrophysiological properties of the cells in the PN slices.

Methods and Materials

Animal Preparation and Surgical Procedure

Male and female Sprague-Dawley rats weighing 200–400 g were purchased from Orient Bio (Kyunggi-do, Korea). The rats were housed in a temperature-controlled (24–26°C) room under a 12-h light/dark cycle (light on at 9:00 A.M.). The animals had free access to food and water. All animal experiments were carried out in agreement with the guidelines of the Laboratory Animal Care Advisory Committee of Seoul National University.

The rats were anesthetized with an anesthetic cocktail (ketamine 75 mg/kg and xylazine 10 mg/kg) administered intramuscularly to their right femoral regions. All surgical operations were performed under general anesthesia. Under deep anesthesia, after abdominal hair was removed with a razor, and the abdomen was incised along the linea alba. The observations of PVs and PNs were performed above the internal organs under a stereomicroscope (OSM-1; Dongwon, Korea). In situ and in vivo stereomicroscopic images of PVs and PNs were recorded from the surface of the organs with a digital camera (Olympus, Japan).

Slice Preparation of PNs

The isolated PNs were kept in ice-cold (4°C) Ca^{2+}-free Krebs solution and continuously oxygenated with gas (95% O_2, 5% CO_2). A 4% low-melting agarose (SeaPlaque; Lonza, Basel, Switzerland) was dissolved at 70°C and poured into a cubic frame (25 × 25 × 25 mm). The isolated BHC tissues were embedded in this cubic frame at 35°C and then rapidly chilled on ice. After the agarose had solidified, the agarose block was fixed onto a slicing chamber with adhesive. Slices of 200-μm thickness were sectioned with a vibrating tissue slicer (Vibratome 1000 Plus; Vibratome, St. Louis, MO). The slices were immediately moved into an incubating chamber containing oxygenated Krebs solution at 31°C (Pillekamp et al. 2005). The composition of the Krebs solution was (in mM): NaCl, 120.35; KCl, 5.9; $NaHCO_3$, 15.5; NaH_2PO_4, 1.2; $MgSO_4$, 1.2; $CaCl_2$, 2.5; and glucose, 11.5 (Spencer et al. 2005).

Electrophysiological Recording

For slice patch recording, a PN slice was transferred to a recording chamber (0.7 ml) and fixed by means of a grid of nylon stocking threads supported by an O-shaped silver wire weight while being continuously perfused (3 ml/min) with oxygenated (95% O_2, 5% CO_2) Krebs solution at 30–33°C. Patch pipettes were pulled from borosilicate glass capillaries of 1.7-mm diameter and 0.5-mm wall thickness. The pipette internal solution contained (in mM) 135 K-gluconate, 5 KCl, 20 HEPES, 0.5 $CaCl_2$, 5 EGTA, and 5 Mg ATP (Han et al. 2010). The pH was adjusted to 7.2 with KOH. For Krebs solution containing tetraethylammonium chloride (TEA), NaCl was replaced with equimolar TEA. Individual PN cells were identified using a light microscope with differential interference contrast (BX50WI, Olympus, Tokyo, Japan) for the whole-cell patch recording. After the target PN cell was selected for recording, the approach of the patch electrode was guided by a three-dimensional micromanipulator (MP-225; Sutter Instruments, Novato, CA). The open resistance of the pipette ranged from 3 to 6 MΩ, and the seal resistances ranged from 1 to 3 Ω. Electrical signals were recorded using an Axoclamp 2B amplifier (Axon Instruments, Foster City, CA). The signals were filtered at 1 kHz and digitized at 10 kHz with an analog-digital converter (Digidata 1320A) and the pClamp program (version 7.0, Axon). RMPs were corrected for the liquid junction potential (∼14.3 mV) in current clamp experiments. The membrane input resistance was calculated by the potential changes (mV) with applied hyperpolarizing current pulses (−60 pA). In voltage clamp recording to classify cell type, currents were activated by a series of depolarizing voltage commands (from −80 mV to +80 mV, in 10-mV increments). The images of PN cells in slice were visualized using a microscope (BX50WI) equipped with CCD camera (VPC-170IR, Japan).

Data Analysis

Experimental data values were expressed as means ± standard errors of the mean (SEM), and error bars are plotted as SEM. Statistical analysis was performed by Student's *t*-test. Further statistical differences among the four groups were investigated with one-way ANOVA and the post hoc Tukey HSD test. *P* values of less than 0.05 and 0.01 were considered statistically significant.

Results

Figure 1a illustrates a typical example of an isolated PN attached to one end of a rat PV (Shin et al. 2005). The primo-vascular tissue was identified in about 70% of the rats used in this study (71 of 101 rats, 68% male and 74% female). The majority of the primo-vascular tissues were observed on the surface of the small and large intestines (77.2%), and the rest were on the surface of the liver (10.5%), spleen (8.8%), and urinary bladder (3.5%). The size of PNs used in this study was $1.53 \pm 0.11 \times 0.8 \pm 0.03$ mm ($n = 57$, mean $\pm$ SE). Under the optical microscope ($\times 200$ to $\times 600$), most cells in the PN slices were round-shaped cells without obvious processes, as shown in Fig. 1b. Some cells were smaller or had the appearance of red blood cells (marked by arrows), and others were larger (marked by asterisks); we did not record these cells. In this study, we focused on the round cells with diameter of ~ 10 μm, which were the most abundant. The mean size of PN cells analyzed in this study was $9.82 \pm 0.12 \times 8.29 \pm 0.09$ μm ($n = 81$, mean $\pm$ SEM).

Passive Membrane Property of PN Cells

The PN cells recorded in this work did not show any significant spontaneous activity at rest; nor did they show action potentials in response to depolarizing current pulses (Fig. 2). The voltage responses were much faster in the PN cells than in the neurons in the hypothalamic paraventricular nucleus (Fig. 2b). The time constant of the voltage response to a hyperpolarizing current pulse was smaller than that of the hypothalamic neuron (3.31 vs. 29.81 ms). The RMP, measured from 39 cells under the whole cell patch clamp configuration, varied widely, from -50 to -10 mV (mean: -36.2 ± 1.68 mV). We did not detect any remarkable correlation between RMP and membrane input capacitance (Fig. 3a), or between RMP and membrane input resistance of these cells (Fig. 3b). In contrast, the input resistances of the PN cells tended to be reduced with the increase in the membrane capacitances (Fig. 3c).

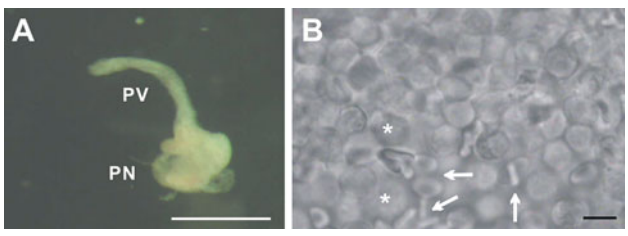

Fig. 1 Preparation of an organ surface primo-vascular tissue for electrophysiological experiment. **a** Isolated PN attached with one end of PV in Krebs solution. Scale bar is 1.0 mm. **b** Cells in a slice (200 μm) of PN for whole-cell recording. *Scale bar* is 10 μm. Most PN cells are round in shape and ~ 10 μm in size, but there were other cells with diameters larger (*asterisk*) or smaller (*arrows*) than 10 μm

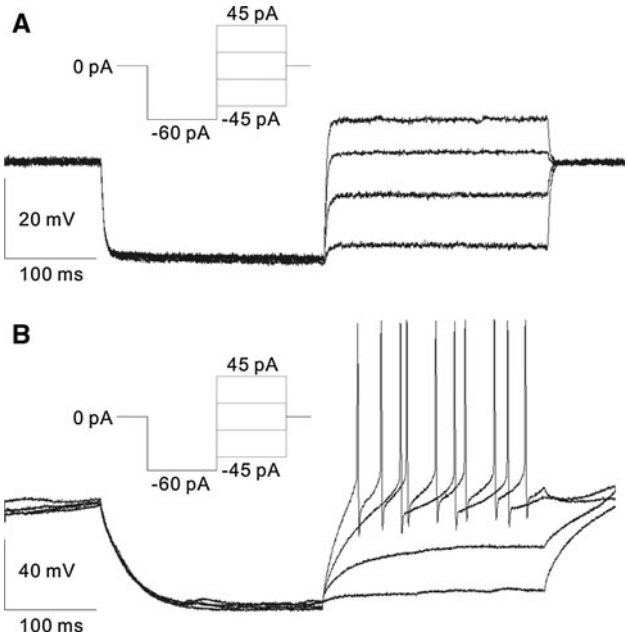

Fig. 2 Representative voltage responses of a PN cell in slice preparation recorded with a patch electrode. Voltage responses of a PN cell (**a**) and hypothalamic neuron (**b**). Current steps applied are shown in *insets*. RMPs were -32 mV (PN cell) and -50 mV (hypothalamic paraventricular neuron). No action potentials were induced in the PN cells

Apparently the round PN cells in the slice appeared similar to the cells in the brain slice. When compared with round hypothalamic neurons in the slice preparation, the RMP and input capacitances of PN cells were significantly smaller than those of neurons ($n = 3$), respectively ($P < 0.001$, Fig. 3d).

Electrophysiological Classification of PN Cells

The data in Fig. 2 indicate that the PN cells are nonexcitable cells. Consistent with this observation, the PN cells in the Krebs solution did not induce any action currents in response to a large depolarizing voltage step (up to 150 mV) in the voltage clamp experiments. On the basis of the current–voltage relations and the presence of time-dependent current as illustrated in Fig 4, the PN cells could be further divided into four types (types I to IV).

Type I PN cells showed large outward current in response to a depolarizing voltage command of 80 mV but very small inward current in response to hyperpolarizing voltage commands of -80 mV from holding potentials of -30 or -40 mV (Fig. 4a). The resulting current–voltage relations show strong outward rectification. Both inward and outward currents were immediately activated in response to the hyperpolarizing and depolarizing voltage commands, respectively. There was no obvious time-dependent activation or inactivation in the current during a

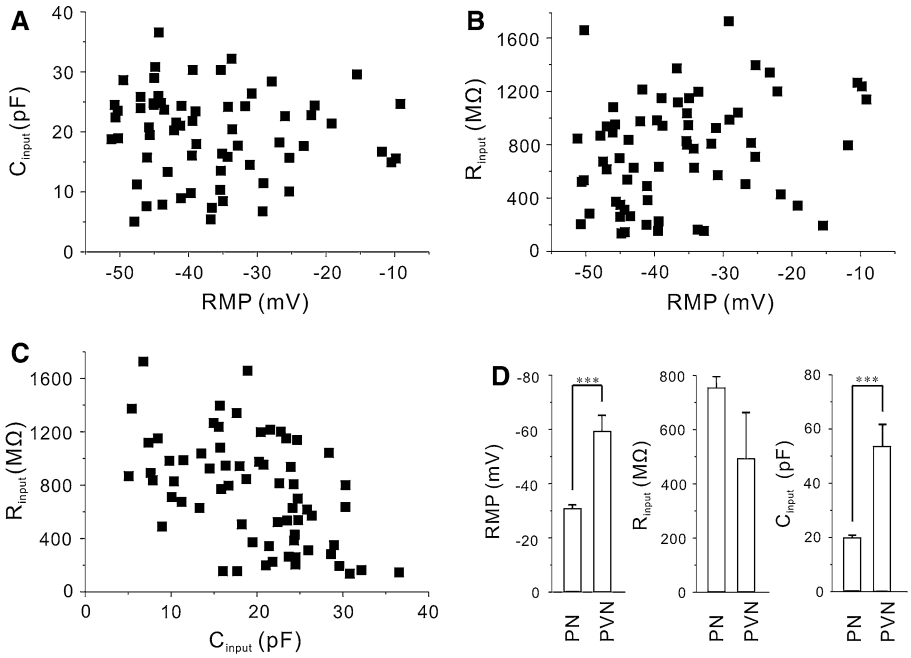

Fig. 3 Passive membrane properties of PN cells recorded with patch electrodes. **a–c** Scatter plots showing correlations between three passive membrane properties: RMP (RMP), input resistance, and input capacitance. **d** Comparison of membrane properties of PN cells with that of neurons from the hypothalamic paraventricular nucleus. ***$P < 0.01$

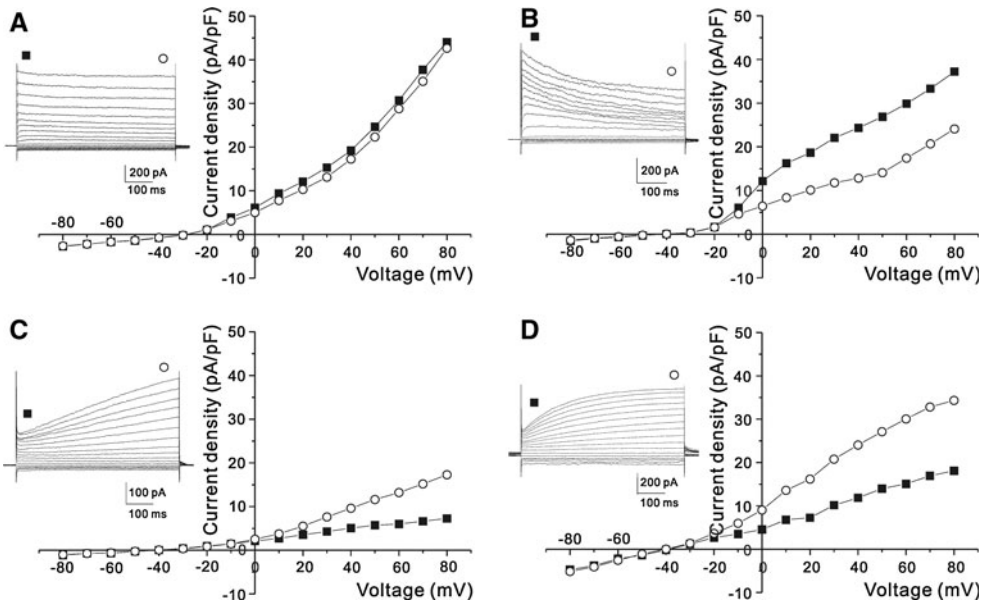

Fig. 4 Four types of current–voltage (I–V) relations recorded from cells in PN slices. I–V curves were obtained by depolarizing step pulses from −80 to 80 mV. **a** Type II–V relations showing an outward rectification. Note that the I–V relations measured at 50 ms (*solid square*) and 550 ms of the 600 ms current pulse (*open circle*) are identical. **b** Type III–V relations showing an outward rectification with a time-dependent activation of outward current. **c** Type III I–V relations showing an outward rectification with a time-dependent and linearly activated outward current. Note lower current density in this cell. **d** Type IV I–V relations showing an outward rectification with a time-dependent and hyperbolic increase in outward current. *Insets* show the current traces for the I–V relations in (**a–d**). Holding potential is −30 (**a**) and −40 mV (**b–d**). The largest outward tail current is seen in current traces of type IV cell. *Scale bars* for insets are 10 μm

voltage command of 600 ms. The type I cells were the majority of PN cells recorded (69%, 45 of 65 cells).

Type II PN cells showed a strong outward rectification in their current–voltage relationships, as in type I cells, but the current decreased by about 36% with time during a voltage step of 600 ms (Fig. 4b). The time-dependent inactivation of outward current was more pronounced with increasing depolarizing voltage command. The type II cells

accounted for 15% of the PN cells recorded (10 of 65 cells).

Type III PN cells were different from type I and type II PN cells: they showed a time-dependent activation of the outward current, which increased more than twofold by the end of a 600-ms voltage command at +80 mV (Fig. 4c). The current density appeared smaller for the type III PN cells than for other cell types (Table 1). Type III PN cells showed a weak outwardly rectifying current–voltage relationship and accounted for 15% of PN cells recorded (10 of 65 cells).

Type IV PN cells (Fig. 4d) were similar to type III PN cells in their outwardly rectifying current–voltage relationship and their time-dependent activation of the outward current. The unique feature of type IV PN cells was in their hyperbolic activation kinetics, which is distinct from that observed in type III cells, which showed a linear activation kinetics in outward current. The activation time constant (τ) of the outward current was obtained by fitting the current traces with the two exponential functions: $f(t) = A_1\exp(-t/\tau_{fast}) + A_2\exp(-t/\tau_{slow})$. A_1 and A_2 are the amplitudes, and τ_{fast} and τ_{slow} are the activation time constants. (Hassfurth et al. 2009). The calculated fast (τ_{fast}) and slow time constants (τ_{slow}) of the outward current in type IV cells were 204 ± 31.0 ms and 67 ± 36.6 ms ($n = 4$, mean ± SE) in the outward current induced by the voltage command to +40 mV. Another unique feature of the type IV cells was its significant outward tail current. Type IV PN cells were least frequently observed (6%, 4 of 65 cells).

Table 1 summarizes the basic electrophysiological parameters of the four types of PN cells. When passive membrane properties were compared, the cells in different types were similar in RMP and input capacitance but different in the input resistance. The input resistance was significantly larger for type II cells (1075 MΩ) than for type I (680 MΩ, $P < 0.05$) and type IV cells (484 MΩ, $P < 0.05$). Because all types of PN cells showed some degree of outward rectification in the current–voltage relationship measured at the end of a 600-ms voltage command, we calculated the amplitude ratio of outward current to inward current induced by the voltage commands of ±40 or ±50 mV from holding potentials, then compared the resulting extent of outward rectifications among the four PN cell types. As shown in Table 1, the rectification ratio was significantly larger for type II cells than for the other three cell types ($P < 0.001$ vs. type I, II, and III). In addition, type III cells showed a significantly lower current density, measured from the current induced by the voltage command to +40 mV, than did type I cells ($P < 0.05$).

Effects of TEA on Membrane Current of Type I PN Cells

Next, we examined the effects of TEA, a nonselective K^+ channel blocker, on the type I PN cells, which were most frequently recorded in the PN slices. As shown in Fig. 5, TEA dose-dependently blocked the whole-cell current of type I cells, and this effect was independent of the membrane potential. At 30 mM, TEA remarkably reduced both inward and outward currents induced by step voltage commands from −80 to +80 mV (Fig. 5a). Figure 5b compares the current–voltage relationships for membrane currents that were sensitive and insensitive to TEA. In seven cells tested, the TEA-sensitive current accounted for about 75%, whereas TEA-insensitive current (the current remaining in 30 mM TEA) was about 25% of the outward current (Fig. 5b). Figure 5c illustrates the whole-cell current at ±60 mV in response to cumulative application of TEA (0–30 mM). The effect of TEA was reversible, and the current was partially recovered during washout period (~10 min, indicated by dotted lines in Fig. 5c). Figure 5d summarizes the inhibitory effect of TEA on both outward and inward currents at +60 and −60 mV, respectively. The inhibitory effects of TEA were similar on inward and outward currents. The concentration of TEA at half inhibition (IC_{50}) of the current was 4.3 ± 1.71 mM for the outward currents recorded at +60 mV and 4.4 ± 1.92 mM for the inward current recorded at −60 mV ($n = 5$, mean ± SEM, $P > 0.05$).

Table 1 Comparison of basic electrophysiological properties of 4 types of PN cells (mean ± SEM)

Cell type (n)	RMP (mV)	Input resistance (MΩ)	Input capacitance (pF)	Rectification ratio	Current density (pA/pF)
I (45)	−37.7 ± 1.52	680 ± 53[a]	20.1 ± 1.17	2.1 ± 0.15[a]	19.73 ± 1.9[a]
II (10)	−38.5 ± 3.17	1075 ± 106[a,b]	17.6 ± 1.77	4.02 ± 0.62[a,b,c]	18.97 ± 2.83
III (6)	−26.0 ± 5.90	990 ± 185	20.1 ± 2.95	1.31 ± 0.18[b]	4.65 ± 0.58[a]
IV (4)	−30.2 ± 1.98	484 ± 126[b]	17.5 ± 0.57	1.52 ± 0.23[c]	6.15 ± 4.48

One-way ANOVA and post hoc Tukey HSD test revealed that input resistance is significantly different between type I and type II ([a]$P < 0.05$) and between type II and type IV ([b]$P < 0.05$), and that the rectification ratio is significantly different between type I and type II ([a]$P < 0.001$), type II and type III ([b]$P < 0.001$), and type II and type IV ([c]$P < 0.01$). The current density (at +40 mV) is significantly different between type I and type III ([a]$P < 0.05$)

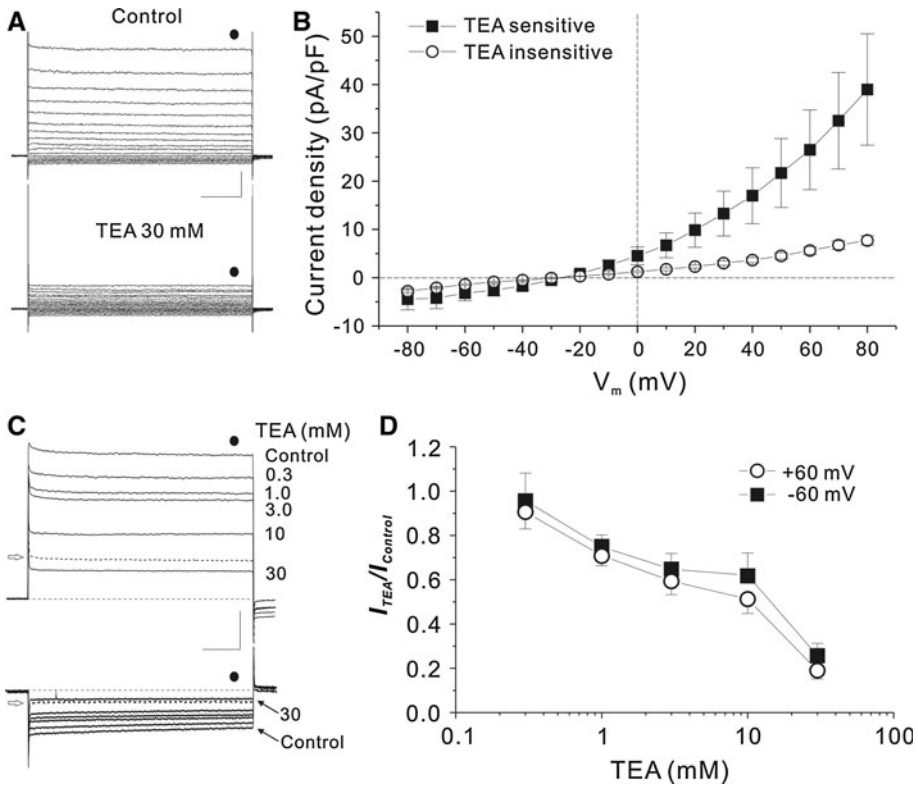

Fig. 5 TEA-induced block of whole-cell current in type I cells. **a** Typical example of the effect of TEA (30 mM) on the whole-cell currents induced by voltage commands from −80 mV to +80 mV in 10-mV increments for 600 ms at holding potential of −30 mV. *Scale bars* are 100 ms and 200 pA. **b** I–V curves for TEA-sensitive and TEA-insensitive currents measured at 550 ms (*solid circles* in **a**). Each point represents means ± SEM from seven cells. The I–V curve for TEA-sensitive current (*solid squares;* difference currents) was obtained by subtracting the current under the action of 30 mM TEA (TEA-insensitive current, *open circles*) from the control currents. **c** Superimposed outward and inward currents in the presence of TEA (0–30 mM). Note a partial recovery marked by *dotted line* and *arrows*. The test current was induced by to 600-ms voltage commands to ±60 mV from a holding potential of −30 mV. **d** Summary graph showing concentration-dependent blockade of the outward and inward currents by TEA. The inward and outward currents measured at 550 ms (*solid circle* in **c**) were normalized to the control current amplitudes. The each point shows the mean ± SEM from five cells

Effects of TEA on Membrane Potential of Type I PN Cells

To determine whether TEA affected the RMP of type I PN cells, we applied TEA to PN cells in current clamp conditions. As shown in Fig. 6a, application of TEA (30 mM) depolarized the membrane potential that was linked with increased membrane resistance. Within about 1 min after bath application of TEA, the membrane potential started to depolarize, and the voltage responses to hyperpolarizing current pulses started to increase as a result of an increase in the membrane input resistance. The effects of TEA on both membrane potential and resistance started to decrease simultaneously, in less than 30 s, after switching to normal Krebs solution. In the washout period, the membrane potential was fully recovered in about 5 min, but the membrane resistance was not fully recovered by the end of the recording (for about 10 min). Figure 6b summarizes the effects of TEA (1, 3, 10, and 30 mM) on the membrane potential, input resistance, and capacitance, which were calculated from the same individual recordings. TEA dose-dependently depolarized the membrane potential (Fig. 6b), and this depolarization was closely correlated with the increase in the membrane input resistances (Fig. 6c). However, the TEA-induced changes in the membrane input capacitances maintained relatively stable (Fig. 6d).

Reversal Potential of Tail Currents of Type I PN cells

The data in Figs. 5 and 6 show that a large proportion of the membrane current in type I cells was blocked by TEA, and that TEA-sensitive conductances contributed to the RMP. To check whether any transient current, such as A-type K^+ current, existed, we compared the whole-cell current induced at holding potentials at −80 mV and −40 mV. As shown in Fig. 7a, no additional current was activated at −80 mV, and the whole-cell current was reversed at −23 mV. To identify whether the outward

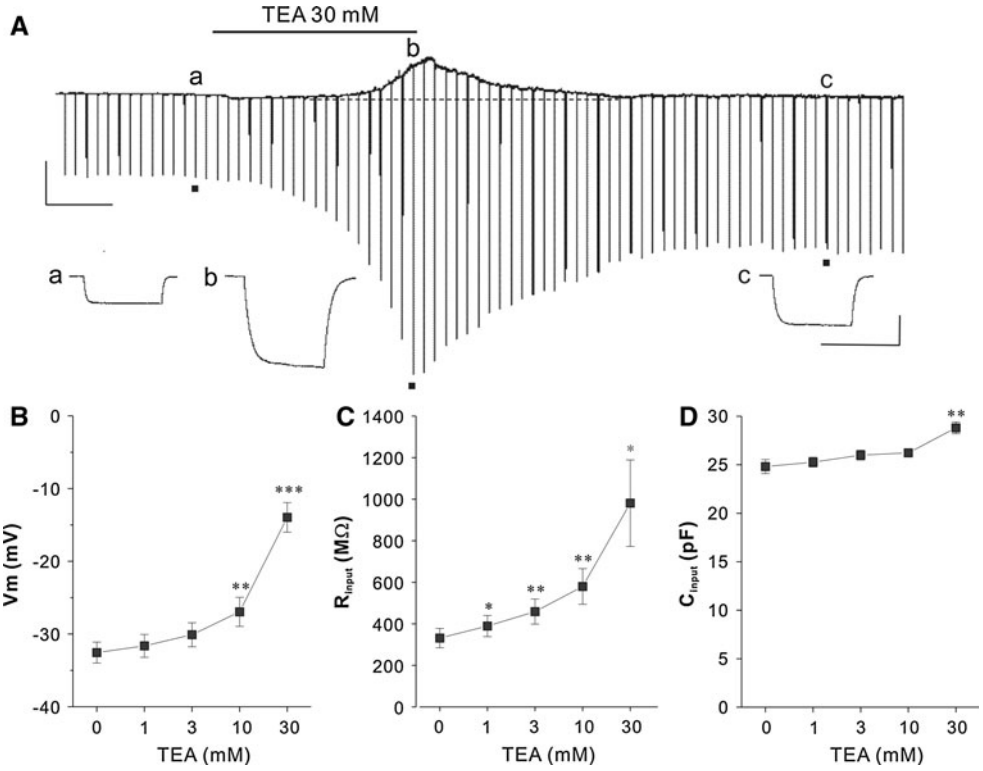

Fig. 6 TEA induced depolarization of the RMP (Vm) measured by whole-cell current clamp recording. **a** Bath perfusion of TEA (30 mM) reversibly depolarized the membrane potential from −32 to −23 mV. TEA also increased membrane voltage responses to hyperpolarizing current pulses (200 ms, −0.1 nA at every 10 s). **a**–**c** Typical examples for downward voltage deflections to hyperpolarizing current pulses before (**a**), during (**b**), and after (**c**) application of TEA. *Scale bars* are 10 mV and 1 min for A, and 20 mV and 0.2 s for the voltage responses (*inset*). Membrane potential and membrane resistance rapidly recovered upon washout of TEA. $*P < 0.05$; $**P < 0.01$; $***P < 0.001$

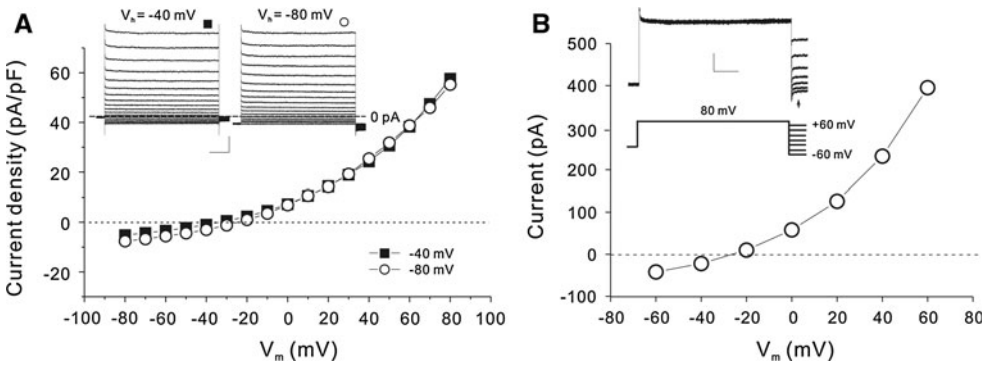

Fig. 7 Reversal potentials of whole-cell current in type I cells. **a** Current–voltage relationships of whole-cell currents (*inset*) induced at holding potentials of −40 and −80 mV in a type I cell. The current amplitudes were measured at the points marked by *solid squares* and *open circles,* respectively. Note the lack of transient outward current at depolarizing voltages from −80 mV and its reversal at −23 mV. *Scale bars* are 100 ms and 400 pA. **b** Current–voltage relationships of the tail currents following a voltage step to +80 mV. The tail current was reversed at −24 mV. Current traces and voltage command protocol between −60 to +60 mV (*inset*). *Scale bars* are 100 ms and 100 p Ape I and type III ($P = 0.018$)

membrane currents activated at depolarized potentials were mediated by K^+-selective channels, we determined the reversal potential of the outward currents (Fig. 7b). In this cell, the tail currents were also reversed at −24 mV (Fig. 7b). In five type I PN cells tested, mean reversal potential of the outward current was -27.0 ± 3.17 mV, which is different from the expected Nernst potential for K^+, −93 mV.

Discussion

The major findings of this study can be summarized as follows: (1) the cells in the PN slices were composed mainly of small and round cells with low RMPs; (2) the PN cells can be grouped into four different types (type I to IV) on the basis of the current–voltage relationships and kinetics of outward current; (3) type I cells, which were

most abundant in the PN slices, expressed a TEA-sensitive current that contributed to its RMP (−36 mV); and (4) the outward current of type I cells was reversed at −27 mV and did not express A-type K^+ current. The results revealed that the PN cells of similar morphology were highly heterogenous in their basic electrophysiological properties. The RMP of the PN in this study (−36 mV) was smaller than those of hypothalamic neurons (−62 mV; Han et al. 2010), retinal neurons (−55 mV for "off" cells and −67 mV for "on" cells; Coleman and Miller 1989), but similar to vascular smooth muscle cells (−34 mV, Guan et al. 2007) recorded using the patch pipettes filled with high K^+ and low Cl^- internal solution. Moreover, this value is similar to the RMP of the PV cells recorded with sharp electrodes (−39 mV; Park et al. 2009). The cells recorded in the present work are similar to the round or oval cells of ∼10 μm with small cytoplasm (Sung et al. 2010). We found that under our experimental conditions, the cells recorded were slightly oval, and their long and short axes were 9.8 and 8.2 μm, respectively. Assuming the cells were spherical, one could estimate the diameter (r) as 12.6 μm by the following relation: $r = [C_i/(4*\pi*C_m)]^{1/2}$, where C_i and C_m are the membrane input (20 pF from Table 1) and specific capacitances (0.01 pF/μm^2), respectively (Kandel et al. 2000). The measured diameter is comparable to the estimated values but smaller than the estimated diameter. The discrepancy might be due to the irregular morphology or the errors in measurement with the light microscope. In addition to the small cells recorded, there are cells with diameters larger than 10 μm (Fig. 1), which is also consistent with the previous report by Sung et al. (2010).

The results of the present study also indicate that a significant proportion (∼75%) of whole-cell current was TEA sensitive (Fig. 5), and that these currents contributed to maintaining the RMP in type I cells (Fig. 6). TEA is a nonselective blocker of K^+ channels including voltage-dependent, Ca^{2+}-activated, ATP-sensitive, and G-protein-activated K^+ channels (Mathie et al. 1998; Eder 1998; Hille 2001). In view of this fact, one would expect a significant expression of K^+ channel current in type I cells. However, the our results did not support this expectation because the tail currents following the outward current evoked by voltage step to +80 mV were reversed at potentials different from the Nernst potential for K^+, −93 mV. The RMP (−36 mV) was also away from the Nernst potential for K^+, −93 mV. Another observation supporting this conclusion was that the effect of TEA was voltage independent (Fig. 5d). If TEA-sensitive current represented a family of voltage-dependent K^+ currents, the effects of TEA should have been more pronounced at the voltages that activate K^+ current at depolarizing voltages. In addition to voltage-dependent K^+ current, TEA is also known to block swelling-activated Cl^- and K^+ conductances (Barrière et al. 2003) as well as voltage-dependent proton channels (Eder and DeCoursey 2001). It is also of note that the kinetics of whole-cell currents in type I cells were similar to the currents reported in these studies. Additional work is needed to gain further understanding of the electrophysiological and molecular properties of TEA-sensitive channels in type I cells.

The PN cells recorded in this study were round in shape (∼10 μm) and low in RMPs (Table 1) without action potentials. The function of these PN cells is as yet unknown. Previous studies showed the presence of monocytes, granulocytes, and small and large lymphocytes in the PN (Lee et al. 2007). The round/oval cells are small in size and are cytoplasm, and hence they are considered to possibly be small lymphocytes or eosinophils (Sung et al. 2010). All these facts strongly suggest that the PN cells recorded in this study are similar to the cells found in the blood.

The proteomics study on the primo-vascular tissues showed that metabolic processes, especially carbohydrate-based ones, were prominent in the primo-vascular tissue. The primo-vascular tissues appear to be equipped with the proteins for an efficient energy supply, which is similar to the findings of proteomic analyses of stem cells, cancer cells, and differentiated myeloid cells that show vigorous proliferation or differentiation (Lee et al. 2008). RMP is known to be smaller in developing, cancerous, or proliferating cells than in developed somatic cells or nonproliferating quiescent cells (see Sundelacruz et al. 2009 for review). Further study is needed to understand whether the active proliferation or maturation of cells occurs in the PN, as suggested by Kim (1965).

In this study, the cells studied were relatively homogenous in morphology: round cells of ∼10 μm in size. They shared the following electrophysiological properties: the RMPs are around −30 mV, and the I–V relationships are outwardly rectifying. In contrast, they were highly heterogenous and could be grouped into four types on the basis of the I–V relationships and the kinetics of the outward current. Presently, it is unknown whether the different types of PN cells represent the different stages of one type of cells under proliferation/maturation (Deng et al. 2007), or whether they are different types of mature cells.

In conclusion, the results of this study showed, for the first time, the basic electrophysiological properties of the small round cells found in PN slices. The PN cells were highly heterogenous in their current–voltage relations and kinetics of outward currents. Our results also indicated that the TEA-sensitive current contributed the RMP in type I cells, but the channels mediating the TEA-sensitive currents appeared different from the most K^+ currents The identification and electrophysiological characterization of

different PN cells could be a fundamental step in further understanding the properties of the primo-vascular system.

Acknowledgements We thank Dr Kwang-Sup Soh for his advice in the course of this work. This work was supported by a grant (2008-0059382) in the Mid-career Researcher Program of NRF funded by the Korean Government (MEST).

References

Barrière H, Rubera I, Belfodil R, Tauc M, Tonnerieux N, Poujeol C, Barhanin J, Poujeol P (2003) Swelling-activated chloride and potassium conductance in primary cultures of mouse proximal tubules. Implication of KCNE1 protein. J Membrane Biol 193: 153–170

Coleman PA, Miller RF (1989) Measurement of passive membrane parameters with whole-cell recording from neurons in the intact amphibian retina. J Neurophysiol 61:218–230

Deng XL, Lau CP, Lai K, Cheung KF, Lau GK, Li GR (2007) Cell cycle dependent expression of potassium channels and cell proliferation in rat mesenchymal stem cells from bone marrow. Cell Prolif 40:656–670

Eder C (1998) Ion channels in microglia (brain macrophages). Am J Physiol 275:C327–C342

Eder C, DeCoursey TE (2001) Voltage-gated proton channels in microglia. Prog Neurobiol 64:277–305

Guan BC, Si JQ, Jiang ZG (2007) Blockade of gap junction coupling by glycyrrhetinic acids in guinea pig cochlear artery: a whole-cell voltage- and current-clamp study. Br J Pharmacol 151: 1049–1060

Han HJ, Sung B, Ogay V, Soh KS (2009) The flow path of alcian blue from the acupoint BL23 to the surface of abdominal organs. J Acupunct Meridian Stud 2:182–189

Han TH, Lee K, Park JB, Ahn D, Park JH, Kim DY, Stern JE, Lee SY, Ryu PD (2010) Reduction in synaptic GABA release contributes to target-selective elevation of PVN neuronal activity in rats with myocardial infarction. Am J Physiol Regul Integr Comp Physiol 299:R129–R139

Hassfurth B, Magnusson AK, Grothe B, Koch U (2009) Sensory deprivation regulates the development of the hyperpolarization-activated current in auditory brainstem neuron. Eur J Neurosci 30:1227–1238

Hille B (2001) Potassium channels and chloride channels. In: Ion channels of excitable membranes, 3rd ed. Sinauer, Sunderland, MA, pp 131–168

Kandel ER, Schwartz JH, Jessell TM (2000) Local signaling: passive electrical properties of the neuron. In: Principles of neural science, 4th edn. McGraw-Hill, New York, pp 140–149

Kim BH (1963) On the Kyungrak system. J Acad Med Sci DPR Kor 90:1–41

Kim BH (1965) Sanal and hematopoiesis (in Korean). J Jo Sun Med 108:1–6

Lee BC, Yoo JS, Ogay V, Kim KW, Dobberstein H, Soh KS, Chang BS (2007) Electron microscopic study of novel threadlike structures on the surfaces of mammalian organs. Microsc Res Tech 70:34–43

Lee SJ, Lee BC, Nam CH, Lee WC, Jhang SU, Park HS, Soh KS (2008) Proteomic analysis for tissues and liquid from bonghan ducts on rabbit intestinal surfaces. J Acupunct Meridian Stud 1:97–109

Lee BC, Bae KH, Jhon GJ, Soh KS (2009) Bonghan system as mesenchymal stem cell niches and pathways of macrophages in adipose tissues. J Acupunct Meridian Stud 2:79–82

Mathie A, Wooltorton JR, Watkins CS (1998) Voltage-activated potassium channels in mammalian neurons and their block by novel pharmacological agents. Gen Pharmacol 30:13–24

Ogay V, Baik KY, Lee BC, Soh KS (2006) Characterization of DNA-containing granules flowing through the meridian-like system on the internal organs of rabbits. Acupunct Electrother Res 31: 13–31

Ogay V, Bae KH, Kim KW, Soh KS (2009) Comparison of the characteristic features of Bonghan ducts, blood and lymphatic capillaries. J Acupunct Meridian Stud 2:107–117

Park SH, Lee BC, Choi CJ, Soh KS (2009) Bioelectrical study of bonghan corpuscles on organ surfaces in rats. J Korean Phys Soc 55:688–693

Pillekamp F, Reppel M, Dinkelacker V, Duan Y, Jazmati N, Bloch W, Brockm-eier K, Hescheler J, Fleischmann BK, Koehling R (2005) Establishment and characterization of a mouse embryonic heart slice preparation. Cell Physiol Biochem 16:127–132

Shin HS, Johng HM, Lee BC, Cho SI, Soh KS, Baik KY (2005) Feulgen reaction study of novel threadlike structures (Bonghan ducts) on the surfaces of mammalian organs. Anat Rec B New Anat 284:35–40

Soh KS (2009) Bonghan circulatory system as an extension of acupuncture meridians. J Acupunct Meridian Stud 2:93–106

Spencer NJ, Hennig GW, Dickson E, Smith TK (2005) Synchronization of enteric neuronal firing during the murine colonic MMC. J Physiol 564:829–847

Sundelacruz S, Levin M, Kaplan DL (2009) Role of membrane potential in the regulation of cell proliferation and differentiation. Stem Cell Rev 5:231–246

Sung B, Kim MS, Lee BC, Yoo JS, Lee SH, Kim YJ, Kim KW, Soh KS (2008) Measurement of flow speed in the channels of novel threadlike structures on the surfaces of mammalian organs. Naturwissenschaften 95:117–124

Sung B, Kim MS, Lee BC, Ahn SH, Hwang SY, Soh KS (2010) A cytological observation of the fluid in the primo-nodes and vessels on the surfaces of mammalian internal organs. Biologia 65:914–918

Yoo JS, Kim HB, Ogay V, Lee BC, Ahn S, Soh KS (2009) Bonghan ducts as possible pathways for cancer metastasis. J Acupunct Meridian Stud 2:118–123